JACS
JOURNAL OF THE AMERICAN CHEMICAL SOCIETY
Communication
pubs.acs.org/JACS

Low-Cost High-Energy Potassium Cathode

Leigang Xue,[†,‡] Yutao Li,[†,‡] Hongcai Gao,[†] Weidong Zhou,[†] Xujie Lü,[§] Watchareeya Kaveevivitchai,[†] Arumugam Manthiram,[†] and John B. Goodenough*[,†]

[†]Materials Science and Engineering Program and Texas Materials Institute, The University of Texas at Austin, Austin, Texas 78712, United States

[§]Earth and Environmental Sciences Division, Los Alamos National Laboratory, Los Alamos, New Mexico 87545, United States

Supporting Information

ABSTRACT: Potassium has as rich an abundance as sodium in the earth, but the development of a K-ion battery is lagging behind because of the higher mass and larger ionic size of K^+ than that of Li^+ and Na^+, which makes it difficult to identify a high-voltage and high-capacity intercalation cathode host. Here we propose a cyanoperovskite $K_xMnFe(CN)_6$ ($0 \le x \le 2$) as a potassium cathode: high-spin Mn^{III}/Mn^{II} and low-spin Fe^{III}/Fe^{II} couples have similar energies and exhibit two close plateaus centered at 3.6 V; two active K^+ per formula unit enable a theoretical specific capacity of 156 mAh g^{-1}; Mn and Fe are the two most-desired transition metals for electrodes because they are cheap and environmental friendly. As a powder prepared by an inexpensive precipitation method, the cathode delivers a specific capacity of 142 mAh g^{-1}. The observed voltage, capacity, and its low cost make it competitive in large-scale electricity storage applications.

The greater abundance and accessibility of Na and K compared with Li prompts investigation of Na-ion and K-ion batteries although the heavier and larger size of the cations makes these batteries less attractive for powering hand-held devices. The cathode of a rechargeable battery is commonly an oxide host into which the working cation is reversibly inserted over a large solid-solution range, but the available high-performance insertion compounds for the larger Na^+ and K^+ cations are limited.

The $M_1M_2(CN)_6$ (M = transition metals) framework of the cyanoperovskite has a large octahedral interstitial space interconnected by open faces bordered by four $C{\equiv}N^-$ anions through which large cations can pass with little disruption of the structure. It has been thoroughly studied as a sodium cathode $Na_2MnFe(CN)_6$,[1,2] which works in an organic electrolyte and has been proven to provide sufficient capacity, voltage, and cycle life at high rates. Working with a liquid K–Na alloy anode at 25 °C, it was observed that Na^+ in $Na_2MnFe(CN)_6$ can be progressively replaced by K^+ due to the lower electrochemical potential of K than that of Na (K^+/K = −2.93 V, Na^+/Na = −2.71 V versus the standard hydrogen electrode), and there is no loss of capacity even though K^+ is bigger than Na^+.[3] This observation shows that $MnFe(CN)_6$ can accommodate about two K^+, which has stimulated the present study on a potassium cathode. $Na_2MnFe(CN)_6$ has been shown to have a small voltage step between two voltage plateaus during the first few cycles; but the step disappears after the initial cycles and is not present if the cathode is vacuum-dried.[1,2] Our $K_xMnFe(CN)_6$ ($x \approx 2$) contains less water than the as-prepared $Na_2MnFe(CN)_6$ and the very small voltage step between the voltage plateaus does not change with cycling. The voltage step in $K_xMnFe(CN)_6$ ($x \approx 2$) is significantly smaller than the 0.6 V step reported in $K_2FeFe(CN)_6$,[4] and the $K_xMnFe(CN)_6$ has a higher voltage.

Another stimulus for a potassium cathode is the recent development of K^+ anode materials. Typical graphitic carbons used in Li-ion batteries do not intercalate Na^+ ions but work with K^+.[5−9] Hard carbons work for both, but they show more promising performance as a K^+ anode.[10] The dendrite-free, liquid K–Na alloy anode acts as a potassium anode.[3] All the above observations tell us to shift some attention to K-ion cells.

The disproportionation reaction $2Mn^{3+} = Mn^{2+} + Mn^{4+}$ prevents the synthesis of a charged $MnFe(CN)_6$ cathode,[11] but the discharged cathode $K_xMnFe(CN)_6$ ($x \approx 2$) can be prepared and cycled electrochemically at room temperature. We prepared $K_xMnFe(CN)_6$ powders by the precipitation method illustrated schematically in Figure 1a$_1$. Analysis of the precipitate by inductively coupled plasma (ICP) gave a K:Fe:Mn molar ratio 1.89:0.92:1. Thermogravimetric analysis (TGA, Figure S1) indicates 4 wt % of water in the powder; corresponding to $K_{1.89}Mn[Fe(CN)_6]_{0.92}{\cdot}0.75H_2O$ (KMHCF), which indicates some $Fe(CN)_6$ vacancies in the structure. The SEM and STEM images (Figure 1a$_2$,a$_3$) show the powder is composed of uniformly distributed nanoparticles with a diameter of about 40 nm, which is much smaller than its sodium analog prepared by the same procedure (140 nm, Figure 1b$_1$,b$_2$,b$_3$), indicating the crystallization rate of potassium manganese hexacyanoferrate is much faster than that of sodium manganese hexacyanoferrate.[12,13] The crystallization rates are so different that only K^+ is precipitated when Na^+ and K^+ coexist with a molar ratio of 1:1 (Figure 1c$_1$,c$_2$,c$_3$, and also see EDS in Figure S2 and XRD in Figure S3). However, the presence of Na^+ induces small primary particles to aggregate and form larger secondary particles with a diameter about 350 nm, resulting in a decreased specific surface area from 50 to 23 m^2 g^{-1}. According to ICP and TGA (Figure S4), the chemical formula of the Na^+-induced potassium manganese hexacyano-

Received: December 7, 2016
Published: January 26, 2017

DOI: 10.1021/jacs.6b12598
J. Am. Chem. Soc. 2017, 139, 2164−2167

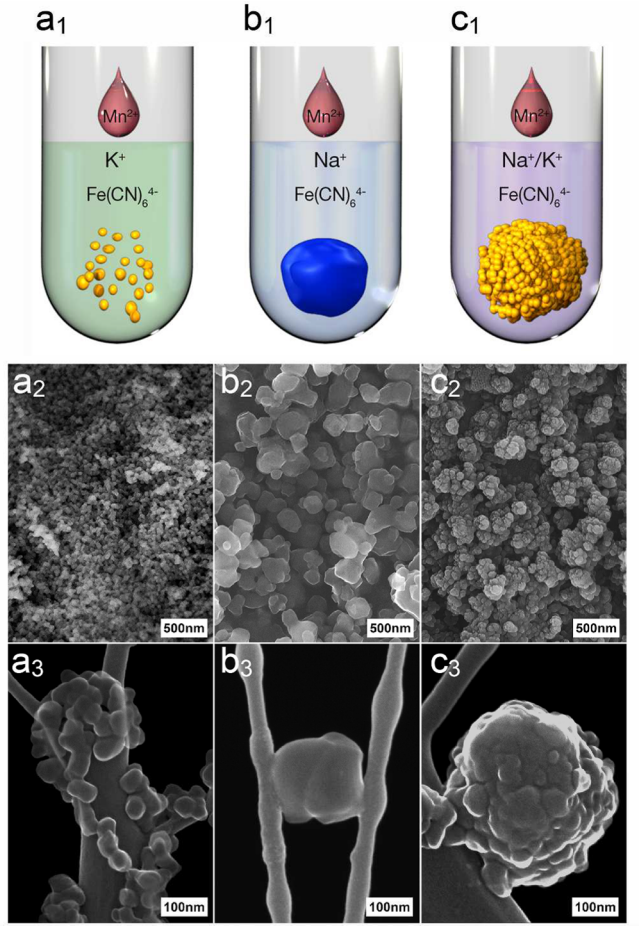

Figure 1. Preparation illustration, SEM and STEM images of (a_1, a_2, a_3) $K_xMnFe(CN)_6$ using K^+ precursors; (b_1, b_2, b_3) $Na_yMnFe(CN)_6$ using Na^+ precursors. (c_1, c_2, c_3) When Na^+ and K^+ coexist with a molar ratio of 1:1 in the solution, only K^+ is precipitated (see EDS, XRD, and ICP), but the 40 nm nanoparticles in diameter aggregate to bigger secondary particles (350 nm) due to a Na^+-induced crystallization. ($x \approx 2$, $y \approx 2$).

ferrate powder is $K_{1.70}Mn[Fe(CN)_6]_{0.90}\cdot 1.10H_2O$ (NI-KMHCF).

The two powders were studied by Synchroton X-ray diffraction (SXRD); the results refined with the fullprof software are shown in Figure 2, S5 and Table S1, S2. Each sample has a monoclinic structure with a similar lattice parameter: a = 6.9770 Å, b = 7.3256 Å, c = 12.2691 Å, and β = 124.5°. The Mn^{2+} and Fe^{2+} ions occupy the Mn—N and Fe—C octahedra, respectively; the high-spin Mn^{III}/Mn^{II} and low-spin Fe^{III}/Fe^{II} couples have similar energies. The 1.88 and 1.72 K^+ ions per formula unit were confirmed in KMHCF and NI-KMHCF from the SXRD, which agrees well with the ICP tests. In Raman spectra of KMHCF and N1-KMHCF between 2000 and 2250 cm^{-1} (Figure S6), three peaks at 2074, 2114, and 2175 cm^{-1}, which correlated to the vibration of $C{\equiv}N^-$ ions and the bonding strength of Fe—C≡N—Mn, were observed; the Fe/Mn ions have the same valence in KMHCF and NI-KMHCF. The magnetic susceptibility (χ) of KMHCF and NI-KMHCF from 2 to 300 K (Figure S7) confirmed the low-spin state of Fe ions and high-spin state of Mn ions. Both KMHCF and NI-KMHCF are paramagnetic and are stable from 2 to 300 K; they have the same calculated effective magnetic moments of 5.9 μ_B per formula. Fe/Mn ions in

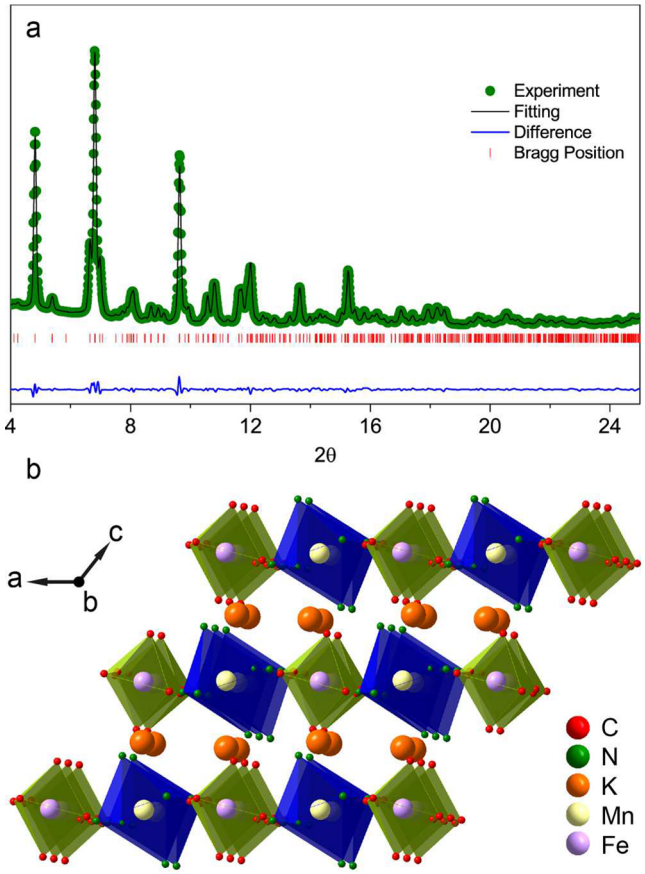

Figure 2. (a) Synchrotron radiation pattern (λ = 0.4246 Å) and Rietveld refinement of $K_{1.89}Mn[Fe(CN)_6]_{0.92}\cdot 0.75H_2O$ powder, and (b) its structural illustration.

KMHCF and NI-KMHCF have the valence of 2, which agrees well with the Raman results.

By using the water-based precipitation method, $MnFe(CN)_6$ hosts more K^+ than Na^+ cations but it absorbs less water with K^+(see the comparison in Table S3); the different ionic sizes and water concentration result in different lattice parameters between $K_xMnFe(CN)_6$ and $Na_yMnFe(CN)_6$; the final K^+/Na^+ cations in the formula unit can be further optimized by tuning the preparation method and water concentration. $K_2MnFe(CN)_6$ has a little lower theoretical capacity than its sodium analog, but it delivers a higher voltage because of the more negative potential of potassium.

To check whether the open faces consisting of four CN^- ions is suitable for reversible K^+ transport between the large K^+ sites inside the $MnFe(CN)_6$ framework, the KMHCF potassium cathode was assembled with a liquid K—Na anode where only K is active in the charge/discharge behavior;[3] a saturated $KClO_4$ in PC containing 10 wt % FEC was used as electrolyte. Upon charge, two plateaus (Figure 3a) at 4.23 and 4.26 V have been observed, corresponding to the successive extraction of two K^+ per formula unit accompanied by the transformations from $K_{1.89}Mn[Fe(CN)_6]_{0.92}$ to $Mn[Fe(CN)_6]_{0.92}$. Upon discharge, two plateaus at 3.60 and 3.56 V correspond to the reverse process. The large polarization mainly results from the low K^+ concentration in the electrolyte;[3,14] the charge voltage would be lower and the discharge voltage would be higher if the polarization could be lowered. The two plateaus at low and high potentials can be assigned to low-spin Fe^{III}/Fe^{II} and high-

DOI: 10.1021/jacs.6b12598
J. Am. Chem. Soc. 2017, 139, 2164–2167

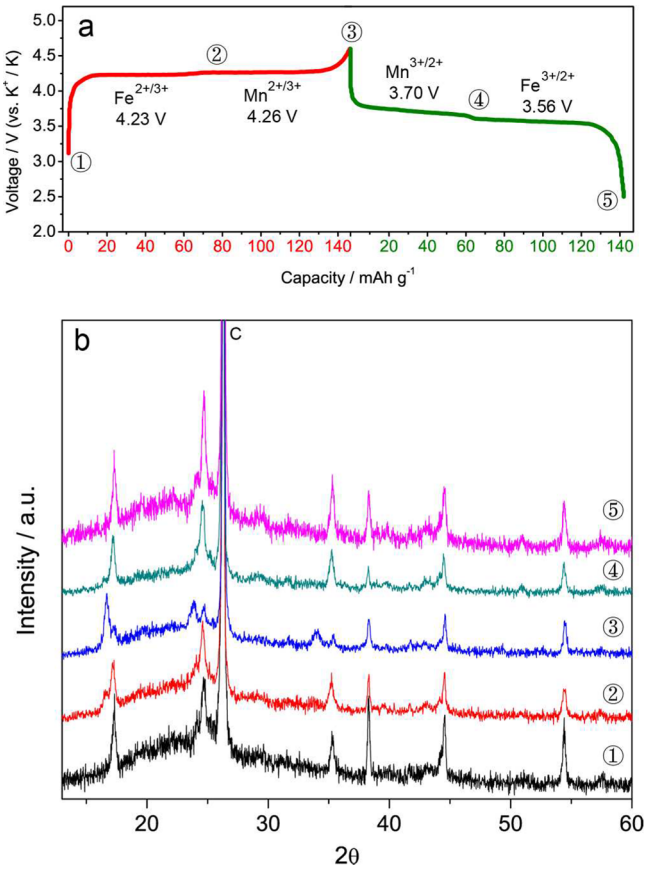

Figure 3. (a) Typical galvanostatic charge/discharge profile of a KMHCF cathode between 2.5 and 4.6 V at 0.2 C. (b) Ex situ XRD patterns to track the structural change upon K^+ extraction and insertion.

spin Mn^{III}/Mn^{II} redox couples, respectively. The capacities of charge and discharge are 146.2 and 142.4 mAh g^{-1} at 0.2 C. The energy difference between the high-spin Mn^{III}/Mn^{II} and low-spin Fe^{III}/Fe^{II} couples is smaller with K^+ than with Na^+.[1] Ex situ XRD was used to track the structural evolution upon K^+ extraction and insertion, as is shown in Figure 3b. Upon K^+ extraction, the growth of new peaks (2θ = 16.7, 24.0, 34.1°) and simultaneous decrease of adjacent existing peaks (2θ = 17.3, 24,7, 35.3°) were clearly observed consistent with a two-phase reaction. Generally, a right shift of peaks and lattice shrinkage happen upon alkali-ion extraction,[2,13,15] but this potassium cathode shows a left shift of peaks and lattice expansion. Because $M_1M_2(CN)_6$ (M = transition metals) has a cubic structure;[16,17] the structural transformation from monoclinic to cubic results in a decrease of β and hence a lattice expansion. Upon K^+ insertion, all the peaks go back to their original states, indicating a good structural reversibility.

From 0.2 to 2 C, the KMHCF potassium cathode shows a capacity retention of 66% (Figure 4a) despite an electrolyte with a low concentration of K^+, indicating the $MnFe(CN)_6$ framework provides fast K^+ insertion/extraction. Both the polarization and the rate capability should be improved further with a stable high-concentration K^+ electrolyte. However, the 40 nm potassium cathode particles show an obvious capacity decay with cycling (Figure 4b and S8). NI-KMHCF powders with larger secondary particles were also tested; they show similar charge/discharge plateaus (Figure 4c) and exhibit more stable cycling performance (Figure 4d). This improvement is to be expected since the current cell has to be charged to 4.6 V due to a big polarization; the 40 nm particles with its high external surface area leads to more side reactions with the liquid electrolyte, especially at high voltage, and hence capacity loss; secondary particles with a larger size and less surface area is proven to be an efficient strategy to improve the cycling performance.[18]

In summary, we have demonstrated that the cyanoperovskite framework $MnFe(CN)_6$ can accept reversibly nearly two K^+ ions as well as two Na^+ ions per formula unit, which means it can also be a rechargeable potassium cathode host with a high theoretical capacity of 156 mAh g^{-1}. The initial cathode has to be in the discharged-state as $K_xMnFe(CN)_6$ ($x \approx 2$) due to the instability of the Mn^{3+} ion. The Fe^{III}/Fe^{II} and Mn^{III}/Mn^{II} redox couples give two flat voltage plateaus around 3.6 V; this voltage should be a little higher after the electrolyte conduction is

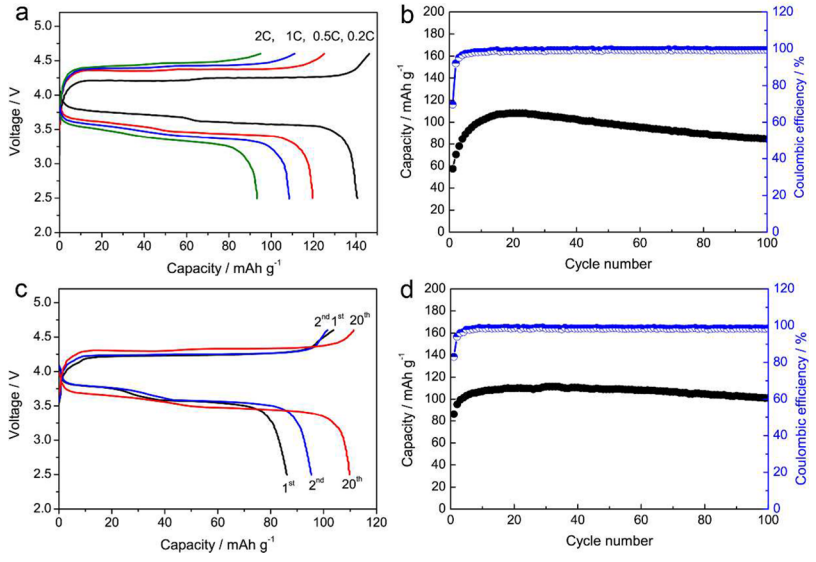

Figure 4. (a) Rate capabilities and (b) cycling performance of KMHCF powder at 1 C. (c) Charge/discharge curves and (b) cycling performance of NI-KMHCF powder at 1 C.

DOI: 10.1021/jacs.6b12598
J. Am. Chem. Soc. 2017, 139, 2164–2167

increased. A V_{dis} = 3.6−4.0 V is a good match to the stability range of existing organic liquid electrolytes.[19,20] The capacity and voltage make it competitive with the mainstream lithium and sodium cathodes such as $LiCoO_2$ (4 V, 140 mAh g^{-1}), $LiFePO_4$ (3.4 V, 170 mAh g^{-1}), and $Na_2MnFe(CN)_6$ (3.4 V, 171 mAh g^{-1}).

■ ASSOCIATED CONTENT

Supporting Information

The Supporting Information is available free of charge on the ACS Publications website at DOI: 10.1021/jacs.6b12598.

Experimental; TGA; XRD; SXRD of NI-KMHCF; Raman spectra; Magnetic susceptibility; Atomic positions (PDF)

Crystallographic details for KMHCF (CIF)

Crystallographic details for NI-KMHCF (CIF)

■ AUTHOR INFORMATION

Corresponding Author

*jgoodenough@mail.utexas.edu

ORCID

Leigang Xue: 0000-0002-7359-7915

Xujie Lü: 0000-0001-8402-7160

John B. Goodenough: 0000-0001-9350-3034

Author Contributions

‡These authors contributed equally.

Notes

The authors declare no competing financial interest.

■ ACKNOWLEDGMENTS

Electrode preparation and testing was supported by U.S. Department of Energy, Office of Basic Energy Science, Division of Materials Sciences and Engineering under award number DE-SC0005397. Optimization of the electrolyte was supported by the U.S. National Science Foundation under award number CBET-1438007. Structural characterization of the cathode was supported by the Lawrence Berkeley National Lab BMR Program under award number 7223523. The authors thank Shaofei Wang for discussion and J. Woznick of the Texas Advanced Computing Center for the art design in Figure 1.

■ REFERENCES

(1) Wang, L.; Lu, Y. H.; Liu, J.; Xu, M. W.; Cheng, J. G.; Zhang, D. W.; Goodenough, J. B. *Angew. Chem., Int. Ed.* **2013**, *52*, 1964.

(2) Song, J.; Wang, L.; Lu, Y. H.; Liu, J.; Guo, B. K.; Xiao, P. H.; Lee, J. J.; Yang, X. Q.; Henkelman, G.; Goodenough, J. B. *J. Am. Chem. Soc.* **2015**, *137*, 2658.

(3) Xue, L. G.; Gao, H. C.; Zhou, W. D.; Xin, S.; Park, K.; Li, Y. T.; Goodenough, J. B. *Adv. Mater.* **2016**, *28*, 9608.

(4) Su, D.; McDonagh, A.; Qiao, S.-Z.; Wang, G. *Adv. Mater.* **2017**, *29*, 1604007.

(5) Jian, Z. L.; Luo, W.; Ji, X. L. *J. Am. Chem. Soc.* **2015**, *137*, 11566.

(6) Komaba, S.; Hasegawa, T.; Dahbi, M.; Kubota, K. *Electrochem. Commun.* **2015**, *60*, 172.

(7) Doeff, M. M.; Ma, Y. P.; Visco, S. J.; Dejonghe, L. C. *J. Electrochem. Soc.* **1993**, *140*, L169.

(8) Kundu, D.; Talaie, E.; Duffort, V.; Nazar, L. F. *Angew. Chem., Int. Ed.* **2015**, *54*, 3431.

(9) Liu, Y. Y.; Merinov, B. V.; Goddard, W. A. *Proc. Natl. Acad. Sci. U. S. A.* **2016**, *113*, 3735.

(10) Jian, Z. L.; Xing, Z. Y.; Bommier, C.; Li, Z. F.; Ji, X. L. *Adv. Energy Mater.* **2016**, *6*, 1501874.

(11) Giri, A.; Goswami, N.; Pal, M.; Myint, M. T. Z.; Al-Harthi, S.; Singha, A.; Ghosh, B.; Dutta, J.; Pal, S. K. *J. Mater. Chem. C* **2013**, *1*, 1885.

(12) Liu, Y.; Qiao, Y.; Zhang, W. X.; Li, Z.; Ji, X.; Miao, L.; Yuan, L. X.; Hu, X. L.; Huang, Y. H. *Nano Energy* **2015**, *12*, 386.

(13) Wu, X. Y.; Wu, C. H.; Wei, C. X.; Hu, L.; Qian, J. F.; Cao, Y. L.; Ai, X. P.; Wang, J. L.; Yang, H. X. *ACS Appl. Mater. Interfaces* **2016**, *8*, 5393.

(14) Peruzzi, N.; Lo Nostro, P.; Ninham, B. W.; Baglioni, P. *J. Solution Chem.* **2015**, *44*, 1224.

(15) Dostal, A.; Kauschka, G.; Reddy, S. J.; Scholz, F. *J. Electroanal. Chem.* **1996**, *406*, 155.

(16) Lee, H. W.; Wang, R. Y.; Pasta, M.; Lee, S. W.; Liu, N.; Cui, Y. *Nat. Commun.* **2014**, *5*, 5280.

(17) Yu, S. J.; Liu, Y. S.; Byeon, S. J.; Park, D. W.; Kim, I. *Catal. Today* **2014**, *232*, 75.

(18) Arico, A. S.; Bruce, P.; Scrosati, B.; Tarascon, J. M.; Van Schalkwijk, W. *Nat. Mater.* **2005**, *4*, 366.

(19) Xu, K. *Chem. Rev.* **2004**, *104*, 4303.

(20) Xu, K. *Chem. Rev.* **2014**, *114*, 11503.

DOI: 10.1021/jacs.6b12598
J. Am. Chem. Soc. 2017, 139, 2164−2167